

Investigation of energetic ion losses induced by long-lived saturated internal mode with energetic particle diagnostics in the HL-2A tokamak

メタデータ	言語: en 出版者: IOP Publishing 公開日: 2023-10-10 キーワード (Ja): キーワード (En): 作成者: ZHANG, Jie, ZHANG, Yipo, CHEN, Wei, CHENG, Shikui, OGAWA, Kunihiro, HE, Xiaofei, WANG, Yongqin, LIU, Yi, XU, Min, ISOBE, Mitsutaka, ZHU, Yuxuan, ZHAN, Xuwen, ZHOU, Jianhang, ZHANG, Jinglong, LIU, Liang, HE, Xiaoxue, LI, Dong, LI, Yonggao, GUO, Wenping, YU, Liming, HAO, Guangzhou, LI, Bo, SHI, Zhongbing, JI, Xiaoquan, ZHONG, Wulv, THE HL-2A Team メールアドレス: 所属:
URL	http://hdl.handle.net/10655/0002000078

This work is licensed under a Creative Commons Attribution 4.0 International License.



PAPER • OPEN ACCESS

Investigation of energetic ion losses induced by long-lived saturated internal mode with energetic particle diagnostics in the HL-2A tokamak






To cite this article: Jie Zhang *et al* 2023 *Nucl. Fusion* **63** 086014

View the [article online](#) for updates and enhancements.

You may also like

- [Fluctuation-induced inward particle flux during L–H transition on HL-2A tokamak](#)
J. Wu, T. Lan, W.X. Ding *et al.*
- [Deformation and fracture of LLM-105 molecular crystals studied by nanoindentation](#)
S O Kucheyev, A E Gash and T Lorenz
- [The ITB dynamics controlled by internal kink modes on HL-2A tokamak](#)
X X He, L W Yan, D L Yu *et al.*

Investigation of energetic ion losses induced by long-lived saturated internal mode with energetic particle diagnostics in the HL-2A tokamak

Jie Zhang¹ , Yipo Zhang^{1,*}, Wei Chen¹ , Shikui Cheng¹, Kunihiro Ogawa^{2,3}, Xiaofei He¹, Yongqin Wang¹ , Yi Liu^{1,*}, Min Xu^{1,*}, Mitsutaka Isebe^{2,3}, Yuxuan Zhu¹, Xuwen Zhan¹, Jianhang Zhou⁴, Jinglong Zhang⁴, Liang Liu¹, Xiaoxue He¹, Dong Li¹ , Yonggao Li¹, Wenping Guo¹, Liming Yu¹ , Guangzhou Hao¹ , Bo Li¹, Zhongbing Shi¹, Xiaoquan Ji¹, Wulv Zhong¹ and the HL-2A Team¹

¹ Southwestern Institute of Physics, PO Box 432, Chengdu 610041, China

² National Institute for Fusion Science, National Institutes of Natural Sciences, Toki, Japan

³ SOKENDAI (The Graduate University for Advanced Studies), Toki, Japan

⁴ College of Nuclear Technology and Automation Engineering, Chengdu University of Technology, Chengdu 610059, China

E-mail: zhangyp@swip.ac.cn, yiliu@swip.ac.cn and minxu@swip.ac.cn

Received 21 February 2023, revised 31 May 2023

Accepted for publication 8 June 2023

Published 23 June 2023



Abstract

Several sets of energetic particle diagnostics, including a set of neutron flux monitoring systems, a solid-state neutral particle analyzer and a fast ion loss probe (FILP), have been used to investigate the energetic ion losses induced by the long-lived saturated internal mode (LLM) in the HL-2A tokamak. Clear experimental evidence for different levels of energetic ion losses induced by LLM, sawtooth and minor disruption has been observed. A numerical calculation for the evolution of neutron emissions was carried out with the FBURN code, and it shows that the neutron emission drop rate linearly increases with the LLM amplitude and no threshold perturbation amplitude exists, illustrating that the loss mechanism for LLM induced energetic ion loss is dominantly convective. In addition, measurement results of the FILP demonstrate that LLM tends to expel energetic ions with relatively low energy ($E < 27$ keV) and high pitch angle ($\theta > 60^\circ$), and can suppress the prompt loss of energetic ions with high energy and low pitch angle to a certain degree. Furthermore, the physical process for LLM induced energetic ion loss can be explained by orbit calculations, which show that LLM induced lost energetic ions will transport from center to peripheral region first, and then get lost out of plasma. The experimental observations are successfully reproduced by calculations using the ORBIT code combined with both the NUBEAM code and the MARS-K code. The paper clearly describes the whole physical process of LLM induced energetic ion loss for the first time in the HL-2A tokamak.

* Authors to whom any correspondence should be addressed.



Original Content from this work may be used under the terms of the [Creative Commons Attribution 4.0 licence](https://creativecommons.org/licenses/by/4.0/). Any further distribution of this work must maintain attribution to the author(s) and the title of the work, journal citation and DOI.

Keywords: energetic ion loss, long-lived saturated internal mode, neutron flux measurement, neutral particle analyzer, fast ion loss probe

(Some figures may appear in colour only in the online journal)

1. Introduction

One of the essential preconditions for achieving self-sustained D-T burning plasma is to confine the energetic ions in fusion plasma long enough to heat the fuel ions [1]. Among the energetic fusion ions in D-T burning plasma, fusion born α particles are of particular interest because they play a vital role in plasma ignition. Actually, energetic ions via auxiliary heating are also important in D-D fusion plasma and allow us to study energetic particle interactions [2]. Hence, it is the inexorable requirement of fusion reactors to achieve excellent confinement quality for energetic ions. Energetic ion losses deteriorate the confinement quality, leading to the reduction of neutral beam injection (NBI) current drive and heating efficiency [3], which is not conducive to the enhancement of the energy gain factor. Furthermore, intense and localized energetic ion loss may damage the plasma facing components, and then cause impurity pollution to the plasma [4]. A small fraction of energetic ion loss in large magnetic fusion devices including ITER might be intolerable [5]. Understanding the behavior of energetic ion loss in fusion plasma is therefore still a crucial issue for fusion research.

Numerous efforts have been made to study the energetic ion loss induced by different magnetohydrodynamic (MHD) instabilities, like toroidal Alfvén eigenmodes (TAEs) [6, 7], energetic particle modes [8, 9], fishbones [10, 11], sawteeth [12] and tearing mode [13]. Investigations of long-lived saturated internal modes (LLMs) observed on many fusion devices [14–17] demonstrate that LLM can eject energetic ions from the plasma core region. The LLM induced energetic ion losses have been observed in MAST with a neutron emission profile monitor [18] and a fast ion loss detector [19]. However, the physical mechanism and process for energetic ion loss induced by LLM are still not sufficiently clear. It should be noted that LLM is a key MHD instability that plays an important role in the advanced scenarios for ITER operation [20], because sustained elevated central safety factor q can be achieved from the action of LLM [21]. Among the advanced scenarios, the hybrid scenario is believed to be a potentially interesting operation scenario for future fusion devices, and many devices such as MAST [14], JET [22], JT-60U [23], DIII-D [24], ASDEX-U [25], EAST [26] and HL-2A [27] have carried out experiments based on the hybrid scenario. Thus, it is of great scientific importance and practical value to investigate the behavior of energetic ion loss induced by LLM.

The present work aims to investigate the physical mechanism and process of energetic ion loss induced by LLM. The experimental setups are described in section 2, in which energetic particle diagnostics including neutron flux measurement (NFM) systems, neutral particle analyzer (NPA) and fast ion loss probe (FILP) are introduced. The experimental results are

shown in section 3. Physical mechanism and process analyses are depicted in sections 4 and 5, respectively. Finally, conclusions are drawn in section 6.

2. Experimental setups

The HL-2A tokamak [28] is a medium-size conventional tokamak with a closed divertor. It has a major radius of 1.65 m, and a minor radius of 0.4 m. The plasma current I_p ranges from 150 to 430 kA, and its orientation is counterclockwise from the top view of HL-2A. The toroidal magnetic field along the magnetic axis B_t , which is mainly created with sixteen toroidal magnetic field coils, ranges from 1.3 to 2.7 T, and is oriented to be clockwise from the top view of HL-2A. The divertor of HL-2A, which is characterized with two closed divertor chambers, enables that it can be operated in either of single-null (SN) and double-null divertor configurations theoretically. However, only lower SN divertor configuration is considered in the present paper.

The NBI system on HL-2A consists of two neutral beam lines, and each beam line is equipped with four positive ion sources. Both beam lines share the same parameters. Each beam line has a maximum injection power of 2 MW. The neutral beam particles have three energy components, i.e. full injection energy E , $E/2$, and $E/3$. Its full injection energy E has a typical value of 40 keV. The neutral beam is injected into the plasma tangentially with a tangency radius of 1.4 m and an angle of 32° with respect to the plasma current along the magnetic axis (see figure 1(a)).

Three kind of energetic particle diagnostics are used to study the behavior of energetic ion loss induced by MHD instabilities, i.e. NFM systems, NPA and FILP. The layout of the energetic particle diagnostics is shown in figure 1(a).

There are two different NFM systems: the one is the ZnS detector, and the other is the ^{235}U fission chamber. The ZnS detector is a newly developed NFM system with an optimum temporal resolution of $1\ \mu\text{s}$ [29, 30]. It is ~ 5 m away from the center of HL-2A. The ZnS detector is sensitive to fast neutrons ($E > 0.7\ \text{MeV}$) rather than slow neutrons and γ/X rays. The ^{235}U fission chamber is a conventional NFM system with a temporal resolution of 1 ms, and it is sensitive to thermal neutrons rather than fast neutrons and γ/X rays. It is ~ 11 m away from the center of HL-2A. Since the fission chamber was calibrated with a ^{252}Cf neutron source, it can be used as a neutron yield measurement system [31].

The NPA system in the present paper is a kind of solid-state NPA [32]. It is located at the low field side in the vacuum chamber and about 15 cm lower than the middle plane. It is equipped with a collimator facing toward the high field side through the plasma core region (see figure 1(b)). An AXUV

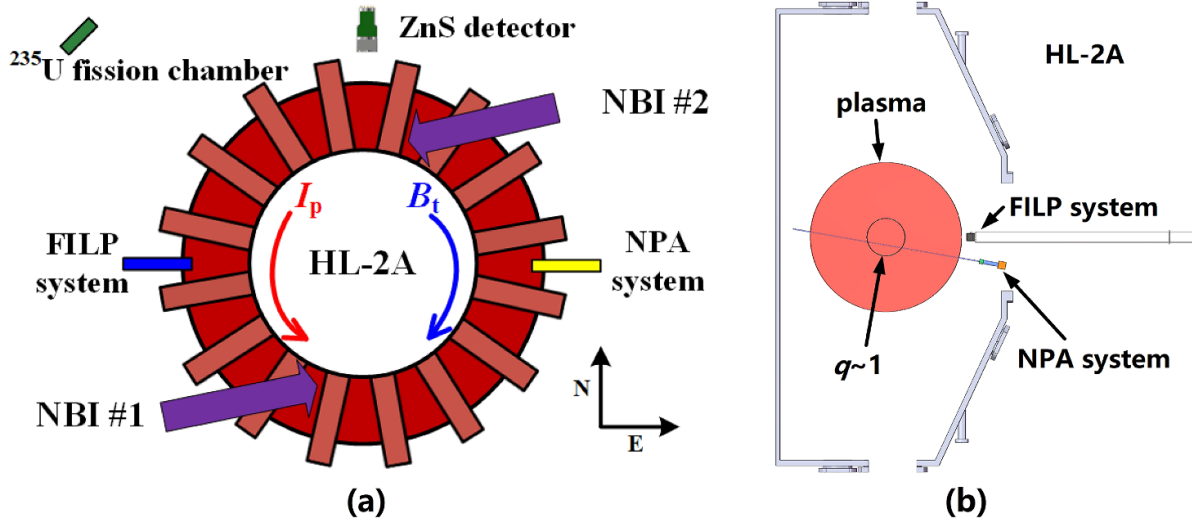


Figure 1. Layout of the NBI system and the energetic particle diagnostics in the planform of HL-2A (a). Plasma current I_p is oriented to be counterclockwise, while toroidal magnetic field B_t to be clockwise. Poloidal view of the NPA system and its sightline, as well as the location of the FILP (b).

silicon photodiode coated with a 100 nm thick tungsten film makes the NPA suitable for measurements of neutral particles with energy over 26 keV generated in the plasma core region. Its sampling rate is 1 MHz. However, the NPA system in the present paper does not have an energy resolution.

The FILP [33] is located at the low field side on the middle plane in the vacuum chamber. Its detector head is ~ 3 cm away from the last closed magnetic flux surface of the HL-2A plasma (see figure 1(b)). The FILP is used to detect the Larmor radius ρ_i of the lost energetic ion as well as its pitch angle θ , from which the energy E_i can be derived: $\rho_i = \frac{\sqrt{2m_i E_i}}{B_i q}$ and $\theta = \arccos(v_{\parallel}/v)$, where m_i , B_i , q , v_{\parallel} , and v are respectively the mass of the lost ion, the local magnetic field at the FILP head, the electrical charge of the lost ion, its velocity parallel to the local magnetic field, and its velocity. The FILP has a temporal resolution of 2 ms.

3. Experimental results

LLM is observed frequently in the HL-2A plasma during NBI with sufficiently high injection power. Figure 2 shows the time traces of some main parameters of an NBI plasma with strong LLMs in which some sawteeth are inserted. An NBI pulse with ~ 0.5 MW in total is injected into the HL-2A plasma from 900 to 1900 ms. The typical value of the plasma current I_p , the central line-averaged electron density n_e and the central electron temperature T_e is about 160 kA, $1.8 \times 10^{19} \text{ m}^{-3}$, and 2.2 keV, respectively. The sampling rates of n_e and T_e are respectively 1 MHz and 30 Hz. A minor disruption occurs at 978 ms, and it has a significant effect on I_p , n_e and T_e . It can be seen from figures 2(c) and (d) that, after the minor disruption, the first LLM appears at ~ 1100 ms and vanishes at ~ 1220 ms, and then several LLMs appears during 1300 ms and 1900 ms together with several sawteeth. This shot makes it possible to investigate the energetic ion losses induced by LLM and sawtooth.

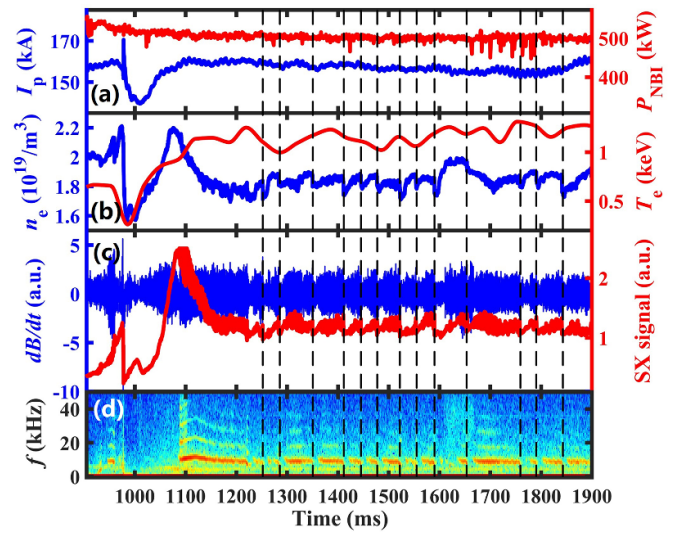


Figure 2. Time traces of the plasma current I_p and NBI power P_{NBI} (a), the line-averaged electron density n_e and electron temperature T_e (b), the magnetic probe signal dB/dt and soft x-ray signal (c), and the frequency spectrogram of the soft x-ray signal (d). LLMs, sawteeth and a minor disruption can be observed in this shot. Dashed vertical lines denote the times of sawtooth crashes (HL-2A # 39020).

In order to characterize the LLM, Bayesian based soft x-ray (SXR) tomography reconstruction [34] for the mode structure has been carried out. The mode structure of LLM at about 1111 ms is shown in figure 3. Both $m/n = 1/1$ mode and $m/n = 2/2$ mode exist simultaneously in the plasma core region, characterizing the existence of LLM [14]. The $m/n = 1/1$ mode with a frequency of ~ 10 kHz and the $m/n = 2/2$ mode with a frequency of ~ 20 kHz can also be observed in the frequency spectrogram of the SXR signal shown in figure 2(d). The normalized minor radius r/a of the $q \sim 1$ surface is estimated to be ~ 0.25 .

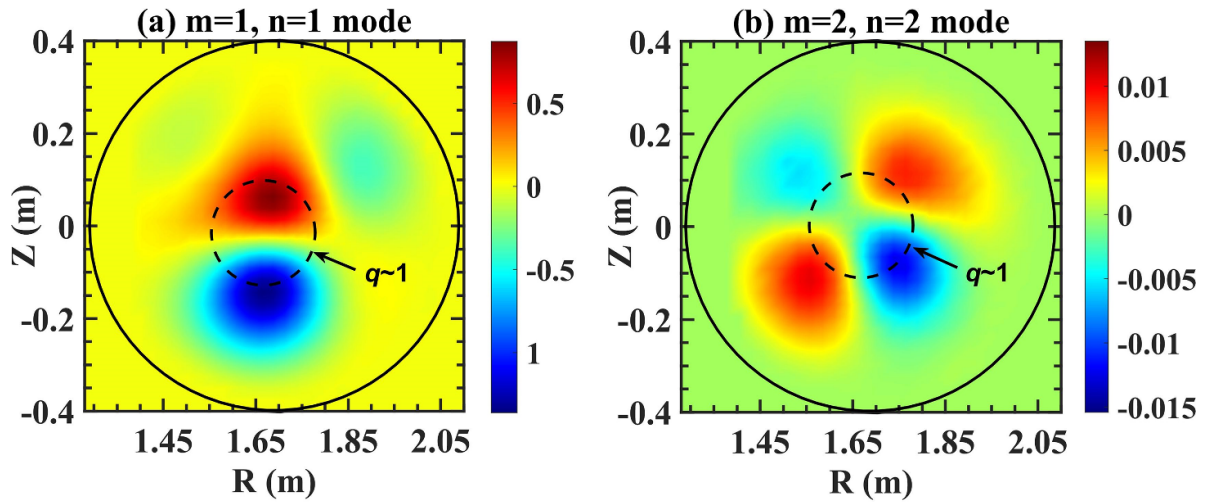


Figure 3. Mode structure of LLM reconstructed by using SXR tomography for shot # 39020. In this shot, $q \sim 1$ surface (dashed circle) has a normalized radius of ~ 0.25 .

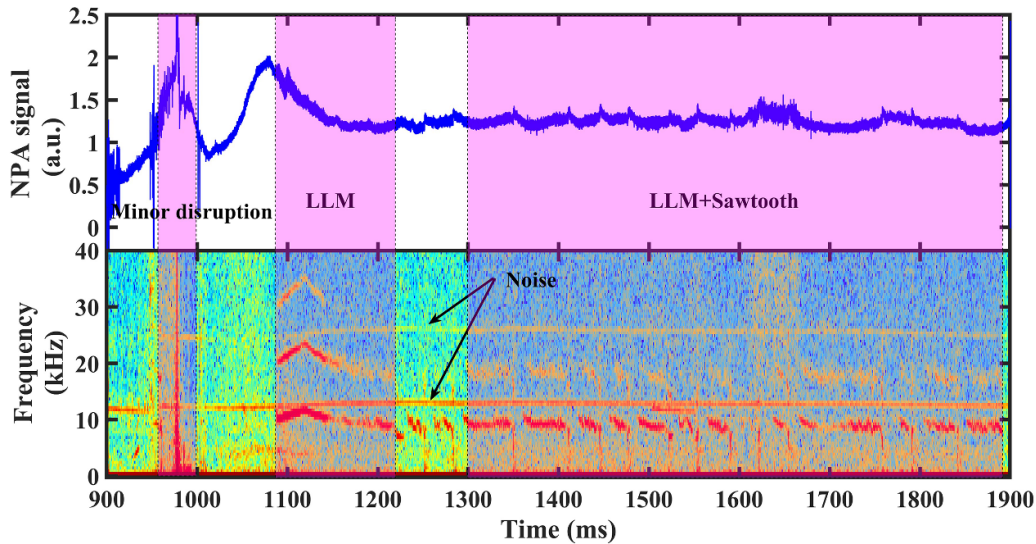


Figure 4. Time traces of the flux of neutral particles with energy over 26 keV (a) and its frequency spectrogram (b). LLMs, sawteeth and a minor disruption can be observed in this shot (HL-2A # 39020).

Since neutral particles exist densely in the plasma peripheral region, energetic ions lost from the plasma core region are likely to become energetic neutral particles via charge-exchange recombination interactions in the plasma peripheral region. Hence, it is possible to study the energetic ion losses in the plasma core region with the NPA system [35, 36]. Figure 4 represents the flux of neutral particles with energy over 26 keV as well as its frequency spectrogram. It can be found that there exist several kinds of MHD instabilities, including mainly minor disruption, LLM and sawtooth. The neutral particle flux responds to minor disruption, LLM and sawtooth, reflecting that all the three MHD instabilities can induce the energetic ion losses.

The emission rate of fusion neutrons is positively associated with the confinement property of the energetic ion population, i.e. the energetic ion loss can lead to the decrease

in neutron yield. To investigate the energetic ion loss behavior, neutron diagnostics can play an important role. The LLM induced energetic ion losses have been observed in different fusion devices indeed by using neutron diagnostics [18, 21]. Figure 5 shows the temporal evolution of neutron emissions measured with both the ^{235}U fission chamber and the ZnS detector.

Both curves respectively measured with the ^{235}U fission chamber and the ZnS detector have the same variation trend, and the deviation between the two curves may attribute to different detection positions (see figure 1). The minor disruption at 978 ms cause a sudden drop in neutron emission. After the minor disruption, a long-lived mode appears. It can be found that the LLM during 1090 ms and 1210 ms induces a slight drop first and then a slight increase in neutron emission, and the drop gets more prominent when sawtooth occurs during

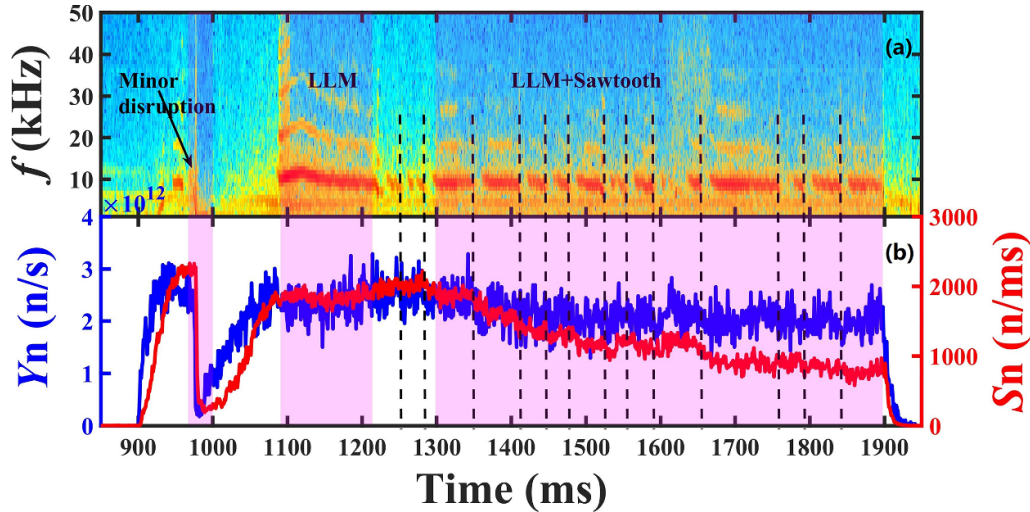


Figure 5. Time traces of the frequency spectrogram of soft x-ray signal (a), and neutron yield Y_n measured with the fission chamber and neutron count rate S_n measured with the ZnS detector (b). Dashed vertical lines denote the times of sawtooth crashes (HL-2A # 39020).

1300 ms and 1900 ms. The slight increase in neutron emission during 1150 ms and 1300 ms might benefit from the reduction in magnetic perturbation amplitude. A prominent continuous decrease in neutron emission is observed during LLM phase inserted with several sawtooth crashes, which was also observed in JET [37].

Since the decrease in neutron emissions may be caused not only by the energetic ion loss but also by the decline in main parameters of the bulk plasma, it is necessary to introduce a precise calculation for the evolution of neutron emissions, which will be described in detail in the next section.

Lost energetic ions can be directly detected by FILPs which have been developed in many fusion devices [38–41]. The energetic ion losses induced by various MHD instabilities have been observed in the HL-2A tokamak by using a FILP [42]. Figure 6 presents the energetic ion losses induced by LLM and/or sawtooth in terms of distribution map measured with the FILP. An NBI pulse with ~ 1 MW in total is injected into the HL-2A plasma during the entire period of the figure. Both LLM and sawtooth can be observed from the SXR signal and its frequency spectrogram.

Four distribution maps in figure 6 depict the energetic ion losses related to prompt loss only (t_1 and t_4), both LLM induced and prompt loss (t_2), and both sawtooth induced and prompt loss (t_3), respectively. Notably, all the distribution maps during the LLM phase are similar to each other. Lost ions are mainly concentrated in three zones in each distribution map, i.e. zone α , β , and γ . Zone α is the region with relatively high energy ($E \sim 40$ keV) and low pitch angle ($\theta \sim 57^\circ$), zone β is the region with relatively low energy ($E \sim 20$ keV) and high pitch angle ($\theta \sim 63^\circ$), and zone γ is the region with relatively low energy ($E \sim 20$ keV) and highest pitch angle ($\theta \sim 75^\circ$). It can be found that the prompt loss of beam ions, which are distributed in zone α and β , dominates the energetic ion loss during NBI. In addition, energetic ion losses

respectively induced by LLM and sawtooth are also observed. The spots for prompt loss at t_1 and t_4 have almost the same brightness and area, while the spots for LLM induced loss at t_2 and sawtooth induced loss at t_3 have higher brightness and larger area especially in the region of relatively low energy and high pitch angle (see zone β and γ). It illustrates that both LLM and sawtooth tend to expel energetic ions with relatively low energy and high pitch angle rather than other cases which are usually caused by other central MHD, such as TAE [43, 44], NTM [45] and TM [42]. For example, TAE is likely to eject energetic ions with relatively high energy ($40 \text{ keV} < E < 180 \text{ keV}$) and low pitch angle ($\theta < 45^\circ$) in LHD [44], and NTM to eject those with comparable energy and relatively low pitch angle ($\theta \sim 40^\circ$) in ASDEX Upgrade [45], compared with beam ions. Our result further verifies the simulation result that sawtooth crashes may provide a mechanism to expel energetic ions with relatively low energy and could be used for He ash removal [46].

4. Physical mechanism for energetic ion loss

Mechanisms for energetic ion loss induced by MHD instabilities can be classified into three categories, characteristics of which are listed as follows [43, 47–49]. The dominant loss mechanism of the first category is convection. It has no threshold perturbation amplitude and does not induce thermal ion loss, and the loss quantity is proportional to the amplitude of MHD modes. The second category is dominantly diffusion. It has a threshold amplitude and the loss quantity varies quadratic with the amplitude of MHD modes. The last category is mainly stochastic process. It has higher perturbation amplitudes than the second category, and energetic ion losses as magnetic field and ion orbits become stochastic. The last category can induce thermal ion losses.

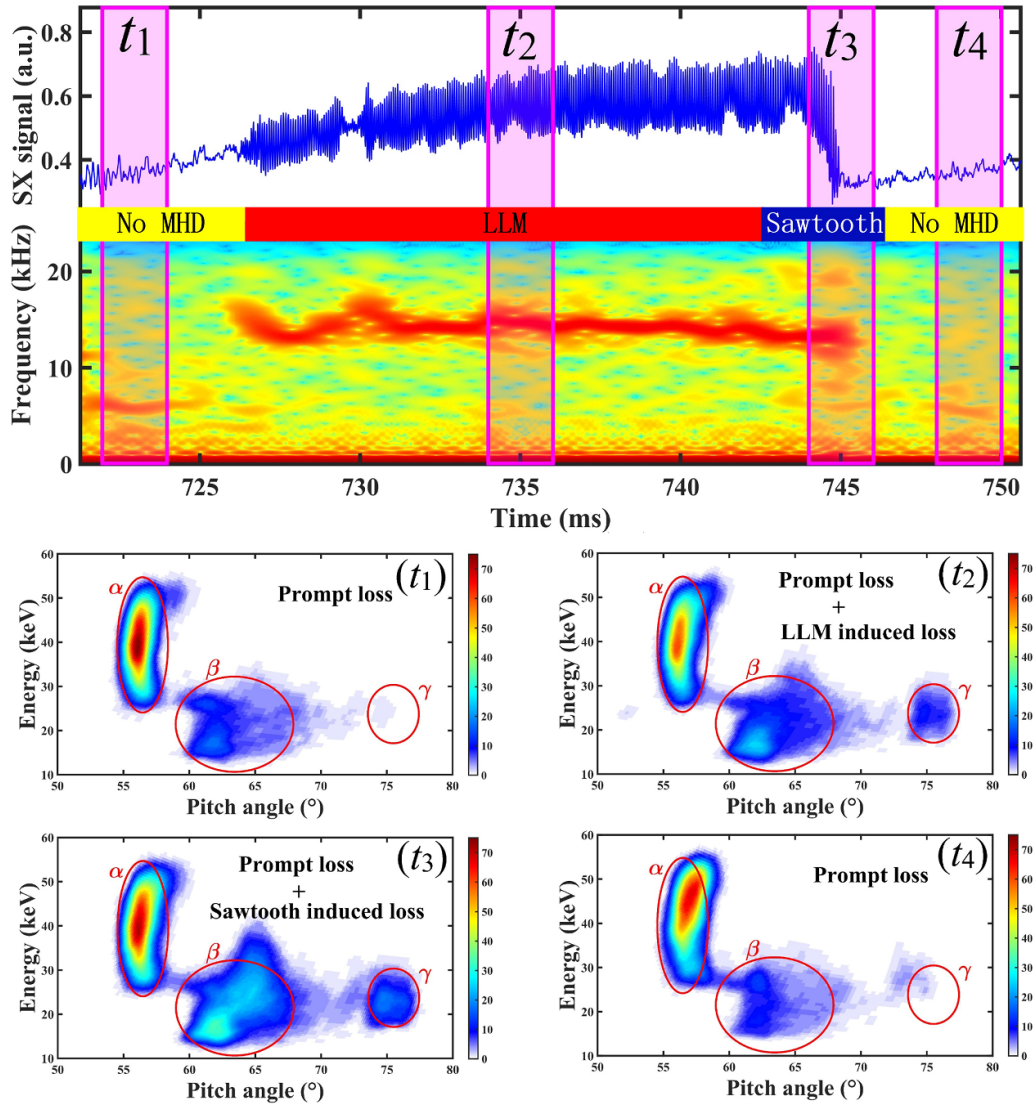


Figure 6. Energetic ion losses induced by LLM and/or sawtooth. The upper panel shows the soft x-ray signal and its frequency spectrogram, with four frame intervals of the FILP labelled with pink rectangles. The distribution maps in the energy-pitch angle plane measured with the FILP are shown in the lower panel, and they depict the energetic ion losses at t_1 (no MHD), t_2 (LLM), t_3 (sawtooth) and t_4 (no MHD), respectively. Lost ions are mainly concentrated in zone α , β , and γ (HL-2A # 22614).

4.1. Neutron emission calculation

To analyze the physical mechanism for energetic ion loss induced by LLM, it is required to find out the relationship between the energetic ion loss rate and the perturbation amplitude of magnetic field. A neutron emission analysis code called FBURN [50] is used to perform a precise calculation for the evolution of neutron emissions. The required input parameters are listed below.

Electron density profile: It is measured with the far-infrared laser interferometer [51]. **Electron temperature profile:** It is measured with the multipoint vertical-Thomson scattering diagnostic [52]. **Ion temperature profile:** It is measured with the charge exchange recombination spectroscopy [53]. **Ion density profile:** The profile of deuteron density is obtained from the equation $n_D = \left(\frac{Z_{\text{eff}} - Z_C}{1 - Z_C} \right) n_e$, where Z_{eff} is the effective plasma charge, Z_C the atomic number of carbon and n_e

the electron density. **Effective plasma charge:** The effective plasma charge measured with the visible bremsstrahlung diagnostic [54] show that $Z_{\text{eff}} \sim 2.5$ before the minor disruption and $Z_{\text{eff}} \sim 4$ after the plasma recovered from the minor disruption. **Neutral beam deposition profile:** The neutral beam deposition profile is calculated using the same method as the neutral beam model of the Simulation of Spectra code [55]. Figure 7 shows the calculated neutral beam deposition profile for shot #39020 with a total NBI power of 0.5 MW. The proportion of the three energy components of neutral beam particles, i.e. E , $E/2$, and $E/3$, is 0.44, 0.39, and 0.17, respectively. The neutral beam deposition profile is peaked at the plasma center, which implies that most neutral beam particles are deposited in the plasma core region.

With the input parameters described above, the FBURN code can calculate the neutron emission profiles, as shown in figure 8. Neutron emission profiles are peaked at the center

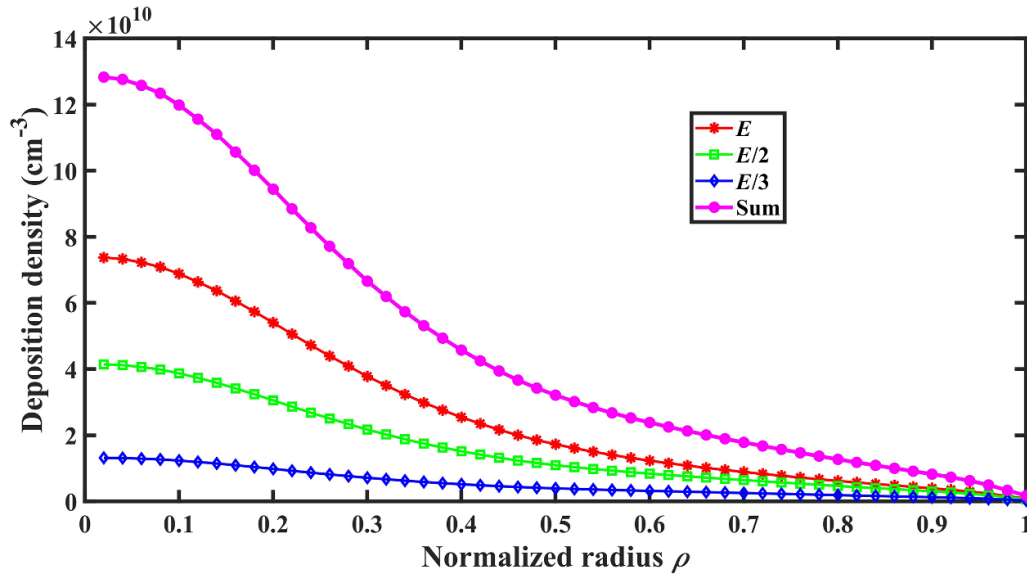


Figure 7. Calculated neutral beam deposition profile. E is the maximum energy of beam particles.

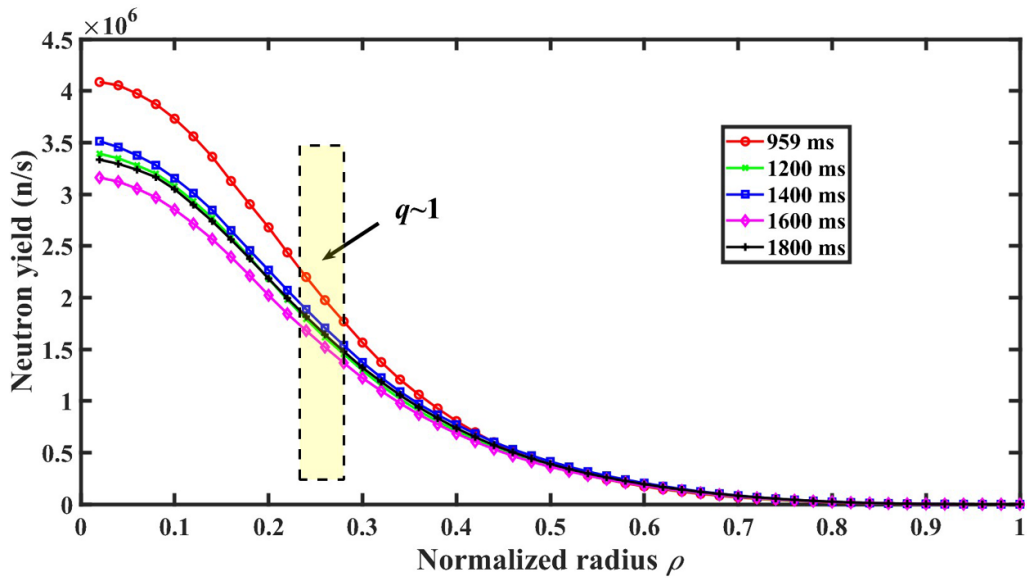


Figure 8. Neutron emission profiles calculated using the FBURN code. The neutron emission profiles are peaked at the plasma center.

as expected, illustrating that fusion reactions mainly occur in the plasma core region. Both LLM and sawtooth occur in the region around $q \sim 1$ surface ($\rho \sim 0.25$). It can be found that the neutron emission profiles are much distinct from each other in the plasma core region with normalized radius $\rho \leq 0.4$, while they are almost indistinguishable in the peripheral region with normalized radius $\rho > 0.4$. It indicates that the energetic ion loss in the MHD active phase mainly occurs within the normalized radius of 0.4.

4.2. Analysis for loss mechanism

The neutron emission evolution curves both measured with neutron diagnostics and calculated with the FBURN code are compared in figure 9. The calculated neutron yield agrees well

with the measurement before 1100 ms, which illustrates that the calculation results are sufficiently accurate. The agreement between calculation and measurement for the minor disruption is due to that FBURN has considered the prominent thermal ion losses induced by the minor disruption at 978 ms. In addition, the deviations between the calculation curve and the experimental curves during LLM and/or sawtooth can be observed after 1100 ms. The FBURN calculation has considered the prompt loss of beam ions without any MHD activities by setting the diffusion coefficient of energetic ions to be $0.2 \text{ m}^2 \text{ s}^{-1}$, which is estimated from neutron emission measurements during MHD quiescent phase. Among its input parameters described above, only the calculated neutral beam deposition profile has a correlation with energetic ions, while other input parameters are associated with the bulk plasma. It

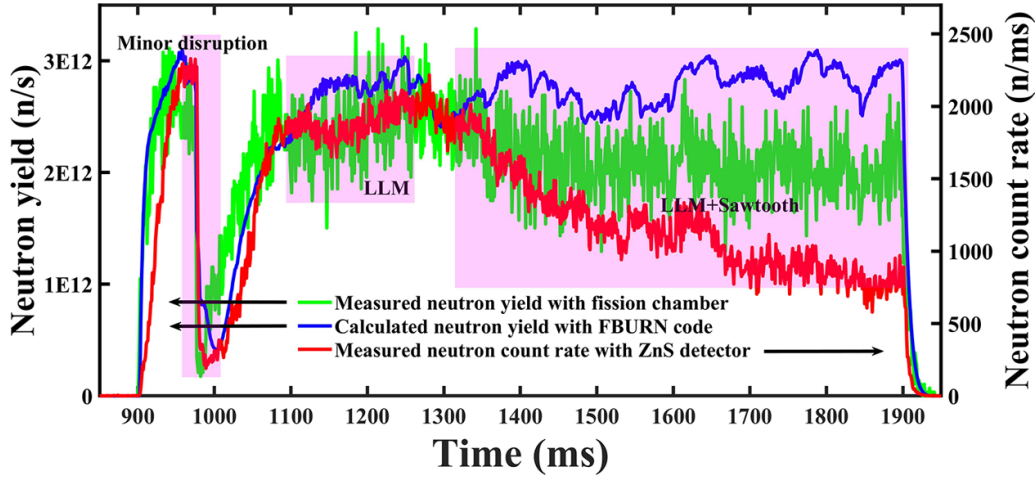


Figure 9. Comparison between the neutron emission evolution curves obtained from experiment and calculation. The deviation between the experimental curves and the calculation curve illustrates that energetic ion loss happens in the period (HL-2A # 39020).

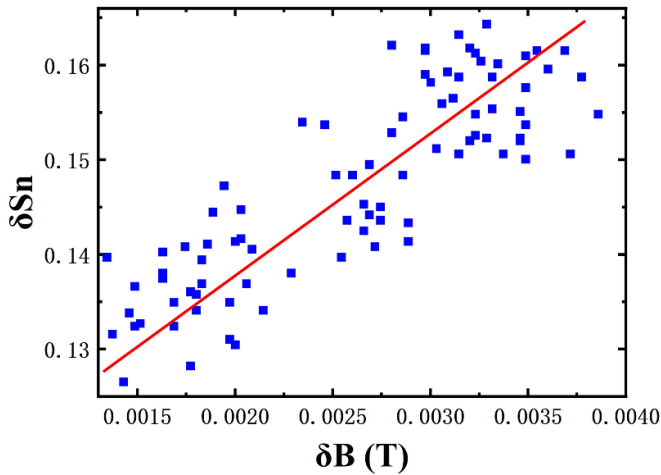


Figure 10. Dependence of the drop rate of total neutron emission rate on LLM amplitude measured by a magnetic probe. δS_n is the drop rate of total neutron emission rate, $\delta S_n = \frac{|S_0 - S_n|}{S_0}$, in which, S_0 is the calculated neutron emission rate, S_n the measured neutron emission rate. δB is the real-time magnetic perturbation amplitude measured with the magnetic probe. The drop rate linearly increases with the LLM amplitude.

should be noted that the anomalous energetic ion loss induced by MHD instabilities is not included. Hence, the deviation between the experimental curves and the calculation curve during LLM and/or sawtooth illustrates that energetic ion loss happens in the period. Comparison between the experimental and calculated neutron emission evolution curves shows that, the LLM during 1090 ms and 1210 ms induces a $\sim 15\%$ reduction in neutron emission, and both the LLMs and sawteeth during 1300 ms and 1900 ms induces more than $\sim 30\%$ reduction in neutron emission.

Figure 10 shows the dependence of the drop rate of total neutron emission rate on LLM amplitude measured by a magnetic probe located on the internal surface of the vacuum vessel. The drop rate of total neutron emission rate linearly increases with the perturbation amplitude, i.e. the energetic

ion loss rate has a positive linear relation on the perturbation amplitude. In addition, it can be found from the positive intercept of the fitting line (the red solid line) that no threshold perturbation amplitude exists in the relation. Both characteristics indicate that the dominant loss mechanism for LLM induced energetic ion loss is convection, which is also the dominant loss mechanism of TAE induced energetic ion loss [43, 47, 56]. The relation between energetic ion loss rate and perturbation amplitude is verified by calculations, which will be discussed in section 5.2.

5. Physical process description for energetic ion loss

5.1. Analysis for energetic ion loss process

Since the energetic ion loss rate is proportional to the light output of the scintillator of the FILP head, the energetic ion loss rate induced by LLM and sawtooth can be estimated from the statistical analyses of the distribution maps in figure 6. Energetic ion loss distribution functions of light output vs. energy and pitch angle are shown in figure 11. Prompt loss is the average of energetic ion loss at t_1 and t_4 . LLM induced loss and sawtooth induced loss are respectively evaluated as the increment of energetic ion loss at t_2 and t_3 from the prompt loss. The LLM induced energetic ion loss is estimated to be 13% of the prompt loss, and the sawtooth induced energetic ion loss is estimated to be 75% of the prompt loss. However, the estimated sawtooth induced loss herein may contain partial or total LLM induced loss. Hence, the estimation value of sawtooth induced energetic ion loss is revised to be 62%–75% of the prompt loss. Since the time scale of LLM is much larger than sawtooth, the energetic ion loss induced by LLM is a mild process that has a much smaller loss rate than prompt loss, while the energetic ion loss induced by sawtooth is a drastic process compared with that induced by LLM. According to the neutron signal, less than 10% neutron yield reduction is observed during the sawtooth crash.

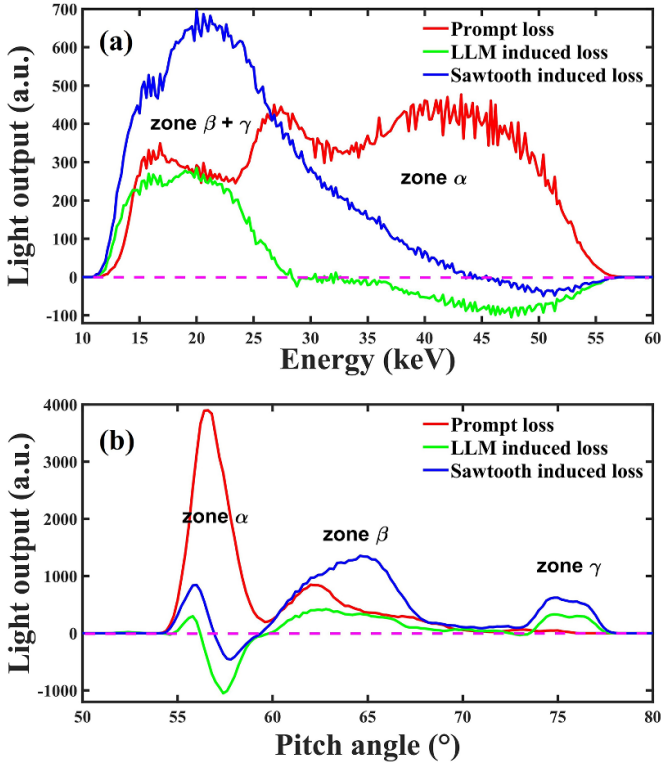


Figure 11. Energetic ion loss distribution functions of light output vs. energy (a) and pitch angle (b). Energetic ion losses induced by LLM and/or sawtooth have relatively low energy and high pitch angles. The negative light output implies that the corresponding prompt loss is suppressed by LLM or sawtooth (HL-2A # 22614).

Figure 11(a) shows that LLM induced energetic ion losses concentrate in zone β and γ , and those induced by sawtooth cover a much wider energy range. It indicates that energetic ion losses induced by LLM have relatively low energy ($E < 27$ keV) compared with the prompt loss. Figure 11(b) shows that both LLM induced and sawtooth induced energetic ion losses concentrate in zone β and γ , i.e. energetic ion losses induced by LLM have relatively high pitch angles ($\theta > 60^\circ$) compared with the prompt loss. Negative light output for the LLM induced loss curve appears during an energy range $37 \text{ keV} < E < 55 \text{ keV}$ and a pitch angle range $56^\circ < \theta < 60^\circ$ (in zone α). It means that the energetic ion losses in zone α during LLM phase are less than the prompt loss, i.e. part of the prompt loss with high energy and low pitch angle is suppressed by LLM, so that the redistribution of energetic ions occurs with the presence of LLM. It is reported that Alfvén instability induced redistribution of energetic ions can reduce the central magnetic shear leading to a reversed shear in a tokamak [57]. It indicates that the redistribution of energetic ions may produce a certain influence to the current redistribution, and even the formation and sustainment of flat or weakly reversed q profiles which are worth studying in the advanced scenarios for ITER operation [21]. Further, it can be speculated that LLM induced energetic ion loss might be related to some observation of internal transport barrier formation during central MHD such as LLM or fishbone, in which poloidal flow is enhanced [58].

The orbits of energetic ions in a magnetic field can be calculated with the following equation, $m_i \frac{d\vec{v}}{dt} = e_i \vec{v} \times \vec{B}$, where m_i is the mass of energetic ion, e_i the charge of energetic ion, \vec{v} the velocity of energetic ion, \vec{B} the magnetic field strength which can be obtained from the equilibrium reconstructed by the EFIT codes [59] combined with the Faraday rotation angle from polarimeter, as well as the constraint of central q -value during sawtooth [60]. The calculated poloidal projections of the lost energetic deuteron ion orbits, which are calculated backward in time from the FILP head, are drawn in figure 12.

Three main components in the distribution maps in figure 6 have been considered in the calculation. For the first component (zone α : $E = 40$ keV, $\theta = 57^\circ$), both trapped and passing particle orbits are observed, and the trapped particle orbits pass through the plasma core region. For the second component (zone β : $E = 20$ keV, $\theta = 63^\circ$) and the third component (zone γ : $E = 20$ keV, $\theta = 75^\circ$), only trapped particle orbits are observed, and all the trapped particle orbits pass through the peripheral region. The first component has a brighter spot because it corresponds to the maximum energy and therefore dominates according to figure 7. Additional magnetic perturbation is introduced to induce anomalous energetic ion losses when MHD instabilities are excited. Since LLM is excited around $q \sim 1$ surface [37] which is shown by the yellow dash circles in figure 12, the energetic ions in the plasma core region are expected to be expelled to the peripheral region via convection as shown by the white arrows in figure 12. For the first component (see figure 12(a)), the lost energetic ions expelled from the plasma core to the peripheral region on the low field side (see the white arrows) have no chance to encounter lost particle orbits. On the contrary, the lost energetic ions expelled from the plasma core to the peripheral region on the low field side (see the white arrows) for the second component (see figure 12(b)) are likely to encounter lost particle orbits and be recorded by the FILP system. It explains why LLM tends to expel energetic ions with relatively low energy and high pitch angle. Please note that the loss orbits of the third component are located at the plasma edge. It illustrates that the energetic ions during LLM instabilities transport from the plasma core region to the peripheral region first, and then being scattered into the loss orbit, which is the same as the energetic ion transport behavior during TAE instabilities [61].

Notably, there exists another possible explanation for the reduced brightness of the main spot during LLM activity. In figure 12(a), both trapped orbits have banana tips located on the high-field side, i.e. their pitch angles are close to precession reversal $\omega_D = 0$. Banana guiding centers of such particles can be trapped by LLM and experience wide (few cm) super-banana oscillations [62]. Such super-banana particles will cross the last closed flux surface well outside the mid-plane, i.e. these loss ions cannot be detected by FILP. In this instance, the conclusion that LLM tends to expel energetic ions with relatively low energy should be relaxed. In order to confirm which explanation is more reasonable, theoretical calculations for LLM induced energetic ion loss is therefore necessary.

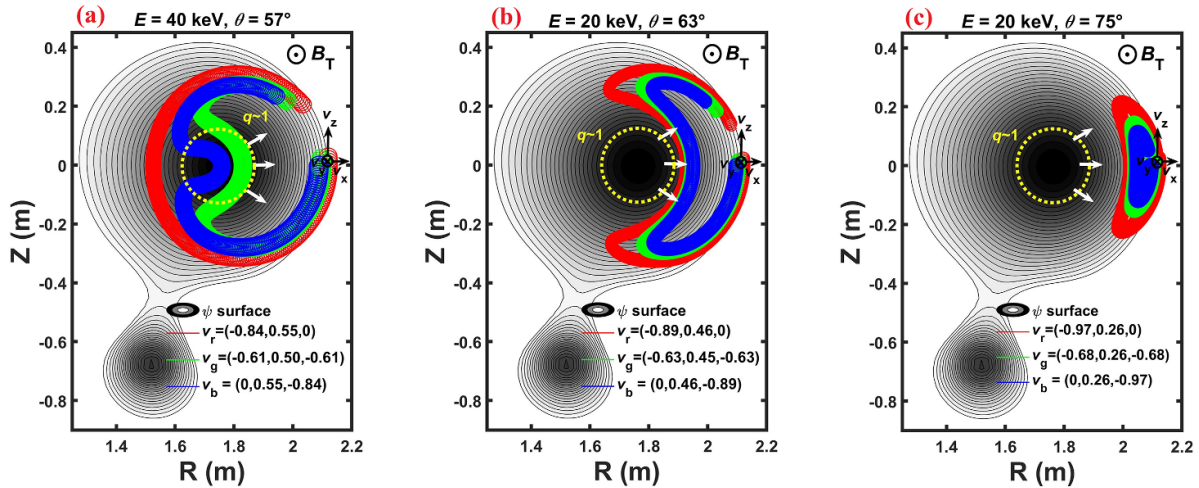


Figure 12. Calculated poloidal projections of the lost energetic deuteron ion orbits. (a) Orbits of deuteron ions with energy $E = 40$ keV and pitch angle $\theta = 57^\circ$ (in zone α); (b) orbits of deuteron ions with energy $E = 20$ keV and pitch angle $\theta = 63^\circ$ (in zone β); (c) orbits of deuteron ions with energy $E = 20$ keV and pitch angle $\theta = 75^\circ$ (in zone γ). Different color represents different velocity direction, v_r , v_g and v_b represent the initial direction vector of the red, green and blue orbit, respectively. ‘ \otimes ’ represents the location of the FILP head.

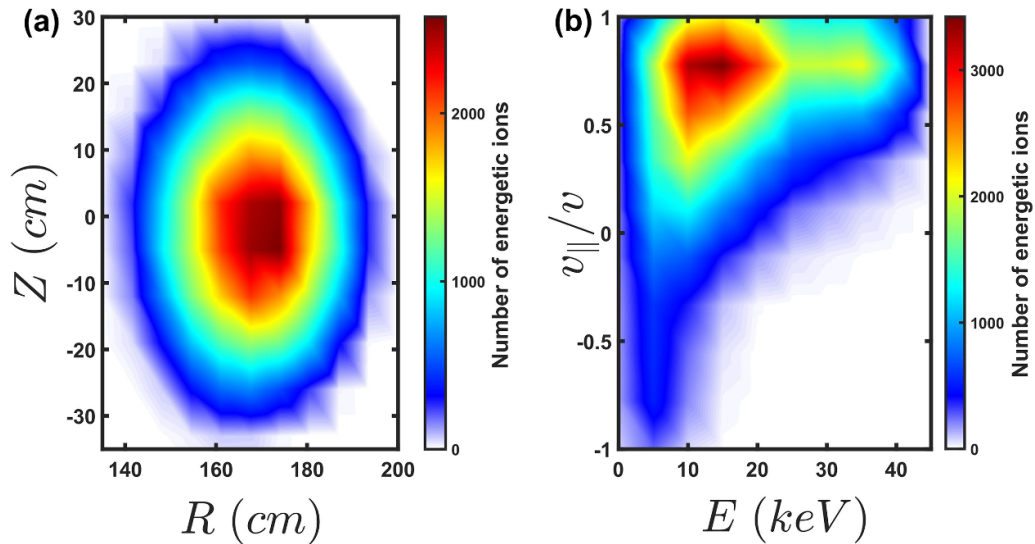


Figure 13. Energetic ion distribution during NBI in HL-2A in (a) real space (R, Z) and (b) phase space ($E, v_{\parallel}/v$) obtained from NUBEAM calculations.

5.2. Theoretical calculations for LLM induced energetic ion loss

To reproduce the experimental observations for LLM induced energetic ion losses, theoretical calculations are carried out. The poloidal profile of energetic ions and the energetic ion distribution in phase space during NBI in the HL-2A tokamak calculated with the TRANSP submodule NUBEAM code [63] are shown in figures 13(a) and (b), respectively. The full energy of neutral beam particles is set to be 45 keV in the calculation. It can be found that the energetic ions have a peaked poloidal profile as expected. Although the full energy component ($E = 40$ keV) dominates the neutral beam deposition profile (figure 7), energetic ions with lower energy ($E < 25$ keV) and forward direction ($v_{\parallel}/v > 0.5$) dominate in the phase space

(figure 13(b)). It can be interpreted as due to the slowing down process of energetic ions in plasma.

In order to calculate the distribution map of lost energetic ions with the ORBIT code [64], the perturbation displacement structure of LLM mode should be input the calculation as a necessary parameter. Figure 14(a) presents the perturbation displacement structure of the LLM mode calculated with the MARS-K code [65]. It can be found that $m = 1$ mode has a prominent perturbation displacement, while $m = 2$ and 3 modes have rather smaller displacements, which can also be seen in figure 2. The perturbation displacement shown by the green curve in figure 14(a) corresponds to the $2/1$ mode, while the second harmonic in figure 2 is the $2/2$ mode. However, since the ratio of the $2/2$ and $1/1$ components is sufficiently small which is estimated to be $\sim 1\%$ according to figure 3, the

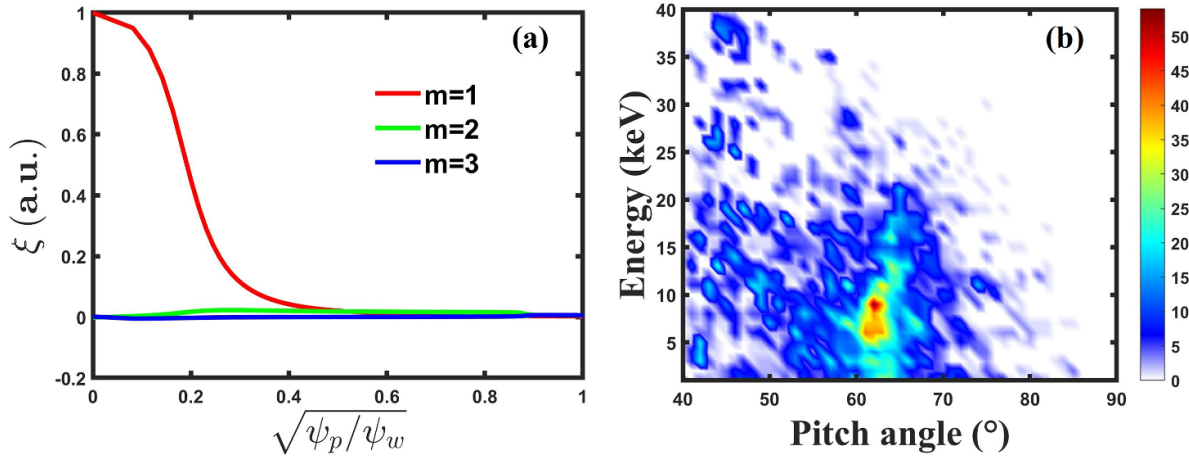


Figure 14. Results of theoretical calculations for shot #39020 at 1111 ms in HL-2A. Figure (a) shows the perturbation displacement structure of LLM mode calculated by the MARS-K code; ξ , ψ_p and ψ_w are respectively the perturbation displacement, the poloidal magnetic flux and the magnetic flux of the last closed flux surface. Figure (b) shows the distribution map of lost energetic ions in the pitch-angle vs. energy plane calculated by the ORBIT code.

discrepancy between calculation and experiment has very limited impact on subsequent ORBIT calculations. Since magnetic probes are located on the vacuum vessel, they cannot measure the absolute mode amplitude of core-localized mode. Herein, we just set the mode amplitude of LLM to be 65 Gs, which is about two times the measured value in figure 10. The factor of 2 is used in the ORBIT simulation here because the mode amplitude of core-localized mode is much higher than the measured value with the edge magnetic probes. Besides the perturbation displacement structure of LLM mode calculated with MARS-K, the ORBIT calculations take the energetic ion distribution calculated with NUBEAM as an input parameter. It should be noted that, unlike the distribution maps of lost ions measured with the FILP, the lost energetic ion in the ORBIT calculations is defined as the energetic ion whose guiding-center can cross the last closed flux surface in 5 ms. The distribution map of lost energetic ions in the pitch-angle vs. energy plane calculated with the ORBIT code is depicted in figure 14(b). The ORBIT calculation here has simulated 500 thousand particle markers. Figure 14(b) shows that lost energetic ions with relatively low energy ($E < 20$ keV) and high pitch angle ($\theta \sim 62^\circ$) are more likely to be expelled during LLM mode. Conversely, lost energetic ions with relatively high energy ($E > 20$ keV) and low pitch angle ($\theta < 60^\circ$) are negligible. Hence, the calculation results are in qualitative agreement with the measurement results, i.e. the experimental observations that LLM tends to expel energetic ions with relatively low energy and high pitch angle are reproduced by the theoretical calculations.

In addition, the dependence of the energetic ion loss rate on the magnetic perturbation amplitude caused by LLM can be obtained from calculations with the ORBIT code, as shown in figure 15. The ORBIT calculations here have simulated 70 thousand particle markers for each magnetic perturbation amplitude. Figure 15 shows that the energetic ion loss rate increases with the magnetic perturbation amplitude linearly, and the intercept of the fitting line (the red solid line) is about

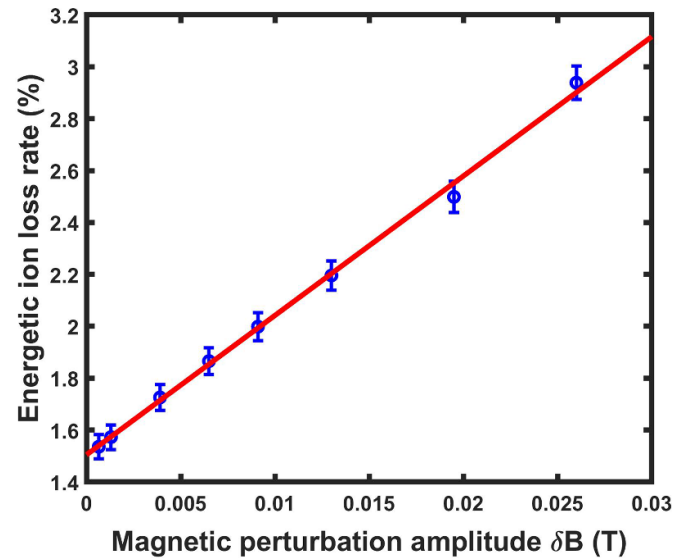


Figure 15. Dependence of energetic ion loss rate on magnetic perturbation amplitude caused by LLM. The energetic ion loss rate increases with the magnetic perturbation amplitude linearly, and no threshold perturbation amplitude for energetic ion loss exists.

1.5%, indicating that no threshold perturbation amplitude exists for LLM induced energetic ion losses. The calculation result has the same linear relation as the experimental result shown in figure 10 which shows that the mechanism for LLM induced energetic ion loss is dominantly convective. However, there is a quite large difference (~ 5 times) between the measured drop of the neutron rate during LLM and the fast ion loss rate calculated by the ORBIT code. There are mainly two aspects of factors for causing the difference. One is that the redistribution of energetic ions is also a significant effect in LLM active plasma in addition to ion loss, which has also been observed in the spherical-torus device [21]. Hence, the measured drop of the neutron rate includes the

contribution of the redistribution of energetic ions. The other is that the ORBIT calculations take the NUBEAM calculation results, which considered the moderated energetic ions, as an input parameter. Notably, the initial beam-born ions suffering prompt loss was not considered in the NUBEAM calculation results. Thus, the fast ion loss rate calculated by the ORBIT code is underestimated, since the ORBIT calculations did not consider the prompt loss of initial beam-born ions.

6. Summary

Energetic ion losses induced by LLM have been measured and investigated in the HL-2A tokamak by means of energetic particle diagnostics, including the NFM systems, the solid-state NPA and the FILP. Measurements show that LLM, sawtooth and minor disruption can lead to varying degrees of energetic ion losses.

Neutron emission calculation has been performed by using the FBURN code with input parameters without considering MHD induced energetic ion losses. Calculated neutron emission profiles show that the energetic ion losses in the MHD active phase mainly occur within the normalized radius of 0.4. The deviation between the neutron emission evolution curves obtained from calculation and experiment illustrates that energetic ion losses are induced by LLM and/or sawtooth. Dependence of the drop rate of total neutron emission rate on LLM amplitude shows that the energetic ion loss rate linearly increases with perturbation amplitude and no threshold amplitude exists in the relation which is verified by the later calculation with the ORBIT code. Hence, the loss mechanism for LLM induced energetic ion loss is dominantly convective.

It is observed with the FILP system that the energetic ion loss induced by LLM is a mild process that has an ion loss rate of 13% of that of the prompt loss. On the one hand, LLM tends to expel energetic ions with relatively low energy ($E < 27$ keV) and high pitch angle ($\theta > 60^\circ$) rather than other cases. On the other hand, LLM can partially suppress the prompt loss of energetic ions with high energy and low pitch angle, indicating that the redistribution of energetic ions and even plasma current may occur with the presence of LLM. The orbit calculations for energetic ions in a magnetic field not only satisfactorily explain the physical process of energetic ion loss induced by LLM, but also show that the lost energetic ions will transport from the plasma center to the peripheral region first, and then get lost out of plasma. In addition, the experimental observations for LLM induced energetic ion losses are also reproduced by theoretical calculations.

Acknowledgments

This work was supported by the National Magnetic Confinement Nuclear Fusion Energy Development Project of China (Grant Nos. 2019YFE03020002 and 2022YFE03040001) and the National Natural Science Foundation of China (Grant Nos. 12205085, 11775068 and 12125502).

ORCID iDs

Jie Zhang  <https://orcid.org/0000-0002-7547-701X>
 Wei Chen  <https://orcid.org/0000-0002-9382-6295>
 Yongqin Wang  <https://orcid.org/0000-0002-3677-7343>
 Dong Li  <https://orcid.org/0000-0003-3746-0839>
 Liming Yu  <https://orcid.org/0000-0002-1177-3063>
 Guangzhou Hao  <https://orcid.org/0000-0003-2310-6134>

References

- [1] Pinches S.D. *et al* 2004 The role of energetic particles in fusion plasmas *Plasma Phys. Control. Fusion* **46** B187
- [2] García-Muñoz M., Fahrbach H.-U., Günter S., Igochine V., Mantsinen M.J., Maraschek M., Martin P., Piovesan P., Sassenberg K. and Zohm H. 2008 Fast-ion losses due to high-frequency MHD perturbations in the ASDEX upgrade tokamak *Phys. Rev. Lett.* **100** 055005
- [3] Forest C.B., Ferron J.R., Gianakon T., Harvey R.W., Heidbrink W.W., Hyatt A.W., La Haye R.J., Murakami M., Politzer P.A. and St John H.E. 1997 Reduction in neutral beam driven current in a tokamak by tearing modes *Phys. Rev. Lett.* **79** 427
- [4] Darrow D.S., Majeski R., Fisch N.J., Heeter R.F., Herrmann H.W., Herrmann M.C., Zarnstorff M.C. and Zweben S.J. 1996 Enhanced loss of fast ions during mode conversion ion Bernstein wave heating in TFTR *Nucl. Fusion* **36** 509
- [5] Heidbrink W.W. and Sadler G.J. 1994 The behaviour of fast ions in tokamak experiments *Nucl. Fusion* **34** 535
- [6] Duong H.H., Heidbrink W.W., Strait E.J., Petrie T.W., Lee R., Moyer R.A. and Watkins J.G. 1993 Loss of energetic beam ions during TAE instabilities *Nucl. Fusion* **33** 749
- [7] Darrow D.S. *et al* 1997 Observations of neutral beam and ICRF tail ion losses due to Alfvén modes in TFTR *Nucl. Fusion* **37** 939
- [8] Bernabei S. *et al* 1999 Role of Alfvén instabilities in energetic ion transport *Phys. Plasmas* **6** 1880–4
- [9] Isobe M. *et al* 2006 Studies of fast-ion transport induced by energetic particle modes using fast-particle diagnostics with high time resolution in CHS *Nucl. Fusion* **46** S918
- [10] Strachan J.D., Grek B., Heidbrink W., Johnson D., Kaye S.M., Kugel H.W., Le Blanc B. and McGuire K. 1985 Studies of energetic ion confinement during fishbone events in PDX *Nucl. Fusion* **25** 863
- [11] Perez Von Thun C. *et al* 2011 Numerical simulation of fast ion loss detector measurements for fishbones on JET *Nucl. Fusion* **51** 053003
- [12] Nave M.F.F., Gorelenkov N.N., McClements K.G., Allfrey S.J., Balet B., Borba D.N., Lomas P.J., Manickam J., Jones T.T.C. and Thomas P.R. 2002 Fast particle effects on the sawtooth stability of JET DT discharges *Nucl. Fusion* **42** 281
- [13] Carolipio E.M., Heidbrink W.W., Forest C.B. and White R.B. 2002 Simulations of beam ion transport during tearing modes in the DIII-D tokamak *Nucl. Fusion* **42** 853
- [14] Chapman I.T. *et al* (MAST Team) 2010 Saturated ideal modes in advanced tokamak regimes in MAST *Nucl. Fusion* **50** 045007
- [15] Gryaznevich M.P. *et al* 2008 Recent experiments on Alfvén eigenmodes in MAST *Nucl. Fusion* **48** 084003
- [16] Manickam J., Pomphrey N. and Todd A.M.M. 1987 Ideal MHD stability properties of pressure driven modes in low shear tokamaks *Nucl. Fusion* **27** 1461

- [17] Wei D. *et al* 2013 Investigation of the long-lived saturated internal mode and its control on the HL-2A tokamak *Nucl. Fusion* **54** 013010
- [18] Cecconello M., Sangaroon S., Turnyanskiy M., Conroy S., Iwona Wodniak R.J.A., Göran Ericsson M.A.S.T.T., Akers R.J. and Ericsson G. 2012 Observation of fast ion behaviour with a neutron emission profile monitor in MAST *Nucl. Fusion* **52** 094015
- [19] Cecconello M. *et al* 2014 Energetic ion behaviour in MAST *Plasma Phys. Control. Fusion* **57** 014006
- [20] Sips A.C.C. *et al* 2005 Advanced scenarios for ITER operation *Plasma Phys. Control. Fusion* **47** A19
- [21] Menard J.E. *et al* 2006 Observation of instability-induced current redistribution in a spherical-torus plasma *Phys. Rev. Lett.* **97** 095002
- [22] McDonald D.C. *et al* 2008 JET confinement studies and their scaling to high β_N , ITER scenarios *Plasma Phys. Control. Fusion* **50** 124013
- [23] Oyama N. *et al* 2009 Long-pulse hybrid scenario development in JT-60U *Nucl. Fusion* **49** 065026
- [24] Petty C.C. *et al* 2015 High-beta, steady-state hybrid scenario on DIII-D *Nucl. Fusion* **56** 016016
- [25] Sips A.C.C. *et al* 2007 The performance of improved H-modes at ASDEX Upgrade and projection to ITER *Nucl. Fusion* **47** 1485
- [26] Gao X. *et al* 2020 Experimental progress of hybrid operational scenario on EAST tokamak *Nucl. Fusion* **60** 102001
- [27] Chen W. *et al* 2022 Recent advances in high- β_N experiments and magnetohydrodynamic instabilities with hybrid scenarios in the HL-2A Tokamak *Fund. Res.* **2** 667–73
- [28] Xu M. *et al* 2019 Overview of HL-2A recent experiments *Nucl. Fusion* **59** 112017
- [29] Zhang J. *et al* 2022 Development of a high-temporal resolution neutron flux measurement system for the HL-2M tokamak *J. Instrum.* **17** 07027
- [30] Zhou J., Zhang J., Zhang J., Zhang Y. and Yang H. 2022 Readout electronics for fast neutron flux measurement with high time resolution on HL-2M tokamak *Fusion Sci. Technol.* **78** 588–94
- [31] Guoliang Y., Zuwei W., Lingfeng W., Zhang J. and Qingwei Y. 2022 Neutron yield measurement system of HL-2A tokamak *Plasma Sci. Technol.* **24** 064006
- [32] Shinohara K., Darrow D.S., Roquemore A.L., Medley S.S. and Cecil F.E. 2004 Solid state neutral particle analyzer array on national spherical torus experiment *Rev. Sci. Instrum.* **75** 3640–2
- [33] Zhang Y.P. *et al* 2014 Development of the scintillator-based probe for fast-ion losses in the HL-2A tokamak *Rev. Sci. Instrum.* **85** 053502
- [34] Li D. *et al* 2016 Bayesian soft x-ray tomography and MHD mode analysis on HL-2A *Nucl. Fusion* **56** 036012
- [35] Medley S.S., Donné A.J.H., Kaita R., Kislyakov A.I., Petrov M.P. and Roquemore A.L. 2008 Invited review article: contemporary instrumentation and application of charge exchange neutral particle diagnostics in magnetic fusion energy experiments *Rev. Sci. Instrum.* **79** 011101
- [36] Polosatkin S., Belykh V., Davydenko V., Fiksel G., Ivanov A., Kapitonov V., Khilchenko A., Khilchenko V., Mishagin V. and Tiunov M. 2011 Advanced neutral particle analyzer for fusion plasma diagnostics *Fusion Sci. Technol.* **59** 259–61
- [37] Bonfiglio P.J., Podesta M., Vallar M., Gorelenkov N.N., Kiptily V., White R.B., Giroud C. and Brezinsek S. (JET Contributors) 2022 Numerical studies on saturated kink and sawtooth induced fast ion transport in JET ITER-like plasmas *Nucl. Fusion* **62** 112002
- [38] Darrow D.S. 2008 Scintillator based energetic ion loss diagnostic for the national spherical torus experiment *Rev. Sci. Instrum.* **79** 023502
- [39] Garcia-Munoz M., Fahrbach H.-U. and Zohm H. (ASDEX Upgrade Team) 2009 Scintillator based detector for fast-ion losses induced by magnetohydrodynamic instabilities in the ASDEX upgrade tokamak *Rev. Sci. Instrum.* **80** 053503
- [40] Zweben S.J. 1989 Pitch angle resolved measurements of escaping charged fusion products in TFTR *Nucl. Fusion* **29** 825
- [41] Isobe M. *et al* 1999 Escaping fast ion diagnostics in compact helical system heliotron/torsatron *Rev. Sci. Instrum.* **70** 827–30
- [42] Zhang Y.P. *et al* 2015 Measurements of fast-ion losses induced by MHD instabilities using a scintillator-based probe in the HL-2A tokamak *Nucl. Fusion* **55** 113024
- [43] García-Munoz M. *et al* 2010 Convective and diffusive energetic particle losses induced by Shear Alfvén waves in the ASDEX Upgrade tokamak *Phys. Rev. Lett.* **104** 185002
- [44] Ogawa K. *et al* 2012 Magnetic configuration effects on TAE-induced losses and a comparison with the orbit-following model in the Large Helical Device *Nucl. Fusion* **52** 094013
- [45] García-Munoz M. *et al* (ASDEX Upgrade Team) 2007 NTM induced fast ion losses in ASDEX Upgrade *Nucl. Fusion* **47** L10
- [46] Bierwage A. *et al* 2022 Energy-selective confinement of fusion-born alpha particles during internal relaxations in a tokamak plasma *Nat. Commun.* **13** 3941
- [47] Garcia-Munoz M. *et al* 2011 Fast-ion transport induced by Alfvén eigenmodes in the ASDEX Upgrade tokamak *Nucl. Fusion* **51** 103013
- [48] White R.B., Goldston R. J., McGuire K., Boozer A.H., Monticello D.A. and Park W. 1983 Theory of mode-induced beam particle loss in tokamaks *Phys. Fluids* **26** 2958–65
- [49] Sigmar D.J., Hsu C.T., White R. and Cheng C.Z. 1992 Alpha-particle losses from toroidicity-induced Alfvén eigenmodes. Part II: Monte Carlo simulations and anomalous alpha-loss processes *Phys. Fluids B: Plasma Phys.* **4** 1506–16
- [50] Ogawa K. *et al* 2018 Time dependent neutron emission rate analysis for neutral-beam-heated deuterium plasmas in a helical system and tokamaks *Plasma Phys. Control. Fusion* **60** 095010
- [51] Li Y. *et al* 2016 Application of the magnetic surface based PARK-Matrix method in the HCOOH laser interferometry system on HL-2A *Plasma Sci. Technol.* **18** 1198
- [52] Huang Y., Wang Y.Q., Hou Z.P., Shang J., Ren L.L., Liu C.H., Feng Z. and Luo C.W. 2019 Recent progress on Thomson scattering diagnostic on HL-2A tokamak *J. Instrum.* **14** C11021
- [53] Wei Y.L. *et al* 2014 High spatial and temporal resolution charge exchange recombination spectroscopy on the HL-2A tokamak *Rev. Sci. Instrum.* **85** 103503
- [54] Liu L. *et al* 2020 Zeff measurement in Ohmic, L- and H-mode plasmas on HL-2A tokamak *IEEE Trans. Plasma Sci.* **48** 2790–8
- [55] Von Hellermann M., de Bock M., Marchuk O., Reiter D., Serov S. and Walsh M. 2019 Simulation of spectra code (SOS) for ITER active beam spectroscopy *Atoms* **7** 30
- [56] Heidbrink W.W., Duong H.H., Manson J., Wilfrid E., Oberman C. and Strait E.J. 1993 The nonlinear saturation of beam-driven instabilities: theory and experiment *Phys. Fluids B: Plasma Phys.* **5** 2176–86
- [57] Wong K.L., Heidbrink W.W., Ruskov E., Petty C.C., Greenfield C.M., Nazikian R. and Budny R. 2004 Internal transport barrier driven by redistribution of energetic ions *Nucl. Fusion* **45** 30

- [58] Deng W. *et al* 2022 Investigation of the role of fishbone activity in the formation of internal transport barrier in HL-2A plasma *Phys. Plasmas* **29** 102106
- [59] Lao L.L., St John H., Stambaugh R.D., Kellman A.G. and Pfeiffer W. 1985 Reconstruction of current profile parameters and plasma shapes in tokamaks *Nucl. Fusion* **25** 1611
- [60] Chen W. *et al* 2019 Resonant interaction of tearing modes with energetic-ions resulting in fishbone activities on HL-2A *Nucl. Fusion* **59** 096037
- [61] Ogawa K. *et al* 2010 Observation of energetic-ion losses induced by various MHD instabilities in the Large Helical Device (LHD) *Nucl. Fusion* **50** 084005
- [62] Marchenko V.S. 1995 Fast ion transport in the $m = 1, n = 1$ kink distorted tokamak central core *Nucl. Fusion* **35** 1155
- [63] Pankin A., McCune D., Andre R., Bateman G. and Kritiz A. 2004 The tokamak Monte Carlo fast ion module NUBEAM in the National Transport Code Collaboration library *Comput. Phys. Commun.* **159** 157–84
- [64] White R.B. and Chance M.S. 1984 Hamiltonian guiding center drift orbit calculation for plasmas of arbitrary cross section *Phys. Fluids* **27** 2455–67
- [65] Liu Y., Ming-Sheng C., Chapman I.T. and Hender T.C. 2008 Toroidal self-consistent modeling of drift kinetic effects on the resistive wall mode *Phys. Plasmas* **15** 112503